

## **Relationship between Building Damage Ratios and Ground Motion Characteristics during the 2011 Tohoku Earthquake**

Hao WU\*  
Kazuaki MASAKI\*\*  
Kojiro IRIKURA\*\*\*  
Koichiro SAGUCHI\*\*\*\*  
Susumu KURAHASHI\*\*\*  
Xin WANG\*\*\*

\*Graduate School of Engineering, Aichi Institute of Technology

\*\*Department of Urban Environment, Aichi Institute of Technology

\*\*\*Disaster Prevention Research Center, Aichi Institute of Technology

\*\*\*\*Department of Environmental Science and Technology,

Interdisciplinary Graduate School of Science and Engineering, Tokyo Institute of Technology

(Received May 1, 2012 Accepted October 1, 2012)

### **ABSTRACT**

Fragility curves, the relationships between three kinds of building damage ratios, i.e., total collapse ratio (TCR), collapse ratio (CR) and damage ratio (DR), as well as ground motion characteristics, i.e., peak ground acceleration (PGA), peak ground velocity (PGV), Japan Meteorological Agency instrumental seismic intensity (IJMA) and spectral intensity (SI), were studied for the 2011 Tohoku Earthquake. It was found that the DR was related better to ground motion characteristics than the TCR and CR during this earthquake, and the correlation between the DR and any one of the PGV, IJMA or SI indices was almost the same. The DR during the 2011 Tohoku Earthquake reached almost the same level as that during the Kobe Earthquake for the same level of ground motions. There were some districts where the DRs did not always correspond to reasonable levels of ground motion characteristics. One reason for this was considered to be the representativeness of the ground motions over each district. Thus, one method of estimating ground motions at damaged sites was proposed by using the underground velocity structures identified from the H/V spectral ratios of microtremors, after we confirmed the consistency of the H/V spectral ratios between earthquakes and microtremors. It is expected to be used for the construction of fragility curves with greater accuracy.

**Keyword:** building damage ratio, ground motion characteristics, underground velocity structure, H/V spectral ratio.

### **1. INTRODUCTION**

The 2011 Tohoku Earthquake on March, 11, 2011 of Mw9.0 was one of the most disastrous mega-

thrust earthquakes in the history of Japan. The rupture was initiated approximately 100 km offshore of Miyagi Prefecture and extended about 450 km in length

and about 200 km in width. During this earthquake, tsunami caused tremendous damage to infrastructures, lifelines, and buildings in the districts along the coastline of the East Tohoku and East Kanto region, and ground shaking also caused significant damage to buildings in the inland districts. According to the Fire and Disaster Management Agency (FDMA, 2012), more than one million buildings were damaged, including those totally collapsed, half-collapsed, and partially damaged due to ground shaking and tsunami as of March 13, 2012. Previous studies (e.g., Miyakoshi et al. 1997; Sakai et al. 2001; Midorikawa et al. 2011; Wang et al. 2011) on the relationship between building damage ratios and ground motion characteristics at stricken districts have been carried out for previous destructive earthquakes. Estimation of ground motions in stricken districts has also been extensively conducted. Take the Kobe Earthquake, for example. Midorikawa and Fujimoto (1996) studied the distribution of the peak ground velocities (PGVs) in and around Kobe City from the overturning of tombstones. Hayashi et al. (1997) evaluated the PGVs from the damage ratios of low-rise buildings. Yamaguchi and Yamazaki (1999) constructed fragility curves based on the relationship between building damage ratios and ground motion characteristics and then estimated the distribution of ground motions at damaged sites with their fragility curves. However, concerning the 2011 Tohoku Earthquake, the relationship between the building damage ratios and ground motion characteristics has not yet been clarified, and estimation of ground motions especially at damaged sites has not been sufficiently investigated.

In this paper, first, fragility curves during this earthquake are constructed based on the relationships between three kinds of building damage ratios, i.e., total collapse ratio (TCR), collapse ratio (CR), and damage ratio (DR), as well as ground motion characteristics, i.e., peak ground acceleration (PGA), peak ground velocity (PGV), Japan Meteorological Agency instrumental seismic intensity ( $I_{JMA}$ ) and spectral intensity (SI) in the stricken districts. Next, the relationship between the building damage ratios and ground motion characteristics during the 2011 Tohoku Earthquake is compared with that during the Kobe Earthquake. Then, we propose a method of estimating ground motions at damaged sites during the 2011 Tohoku Earthquake using the underground velocity

structures beneath the damaged sites and the observed ground motions at strong-motion stations near these sites. Fragility curves with greater accuracy are expected to be constructed with the building damage ratios and estimated ground motion characteristics at damaged sites within each stricken district, as long as the ground motions can be estimated correctly.

## 2. DATA SOURCE

### 2.1 Damage Data

During this earthquake, buildings in coastal districts were mainly damaged by tsunami over the Tohoku and Kanto areas. At the same time, in the inland districts, numerous buildings were damaged by ground shaking. The building damage statistics, i.e., the numbers of totally collapsed, half-collapsed, and partially damaged buildings in the stricken districts, are obtained from the FDMA (2012). The total numbers of buildings in stricken districts are obtained from the Statistics Bureau and Director-General for Policy Planning of Japan (STAT, 2008). The administrative unit of the stricken districts is city, town, or village (*shi, cho, or mura* in Japanese). According to the FDMA, total collapse denotes buildings whose basic functions have been lost for the residents, i.e., the buildings are totally collapsed, washed away, or buried, or the damage to the buildings cannot be recovered through repair. Half collapse denotes buildings whose basic functions for residents have been partly lost for the residents, i.e., the buildings can be recovered through repair. Partial damage means that the damage to buildings is not heavier than total and half collapse, but that the buildings need repair. Slight damage such as cracks on several panes of glass is not classified as partial damage. On the other hand, because our objective is to elucidate damage by ground shaking, districts damaged by tsunami were excluded from the inundation maps provided by the Geospatial Information Authority of Japan (GSI, 2011). At the same time, according to a liquefaction survey report from the Ministry of Land, Infrastructure, Transport and Tourism and the Japanese Geotechnical Society (2011), districts such as Urayasu City, Chiba City and Katori City are significantly affected by liquefaction. They are also excluded. On the other hand, some stricken districts in which strong-motion stations have not been installed are included as long as they

satisfy two conditions (a) and (b): (a) the geology of the stricken districts to be included is similar to that of adjacent stricken districts in which strong-motion stations have been installed; (b) the distance between the building-concentrated street in the district to be included and the strong-motion station in the adjacent stricken district is less than 10 km.

Fig. 1 shows all the stricken districts in the six prefectures along the Pacific east coast. The yellow districts are the stricken ones in which a couple of strong-motion stations are installed. The green districts are those included under the above two conditions. The gray districts are excluded as they are mainly damaged by tsunami. The red districts are also excluded as they are significantly affected by liquefaction. The shadowed districts with slashes are those lacking damage statistics.

## 2.2 Strong-motion Data

The strong-motion records at the K-NET and KiK-net stations were open to the public soon after this earthquake. In this study, the observation records in 72 K-NET stations and 25 KiK-net stations are used to analyze ground motion characteristics. The locations of the K-NET or KiK-net stations in the stricken districts are shown in Fig. 1. The solid triangles represent K-NET stations and the solid circles represent KiK-net stations. For those districts in which there is more than one strong-motion station, the average observed ground motion characteristics at all of the strong-motion stations are taken as the ground motion characteristics for the entire district. In addition, the ground motion record at the Tsukidate station in Kurihara City is not included in the following analysis, because the partial uplifting of the

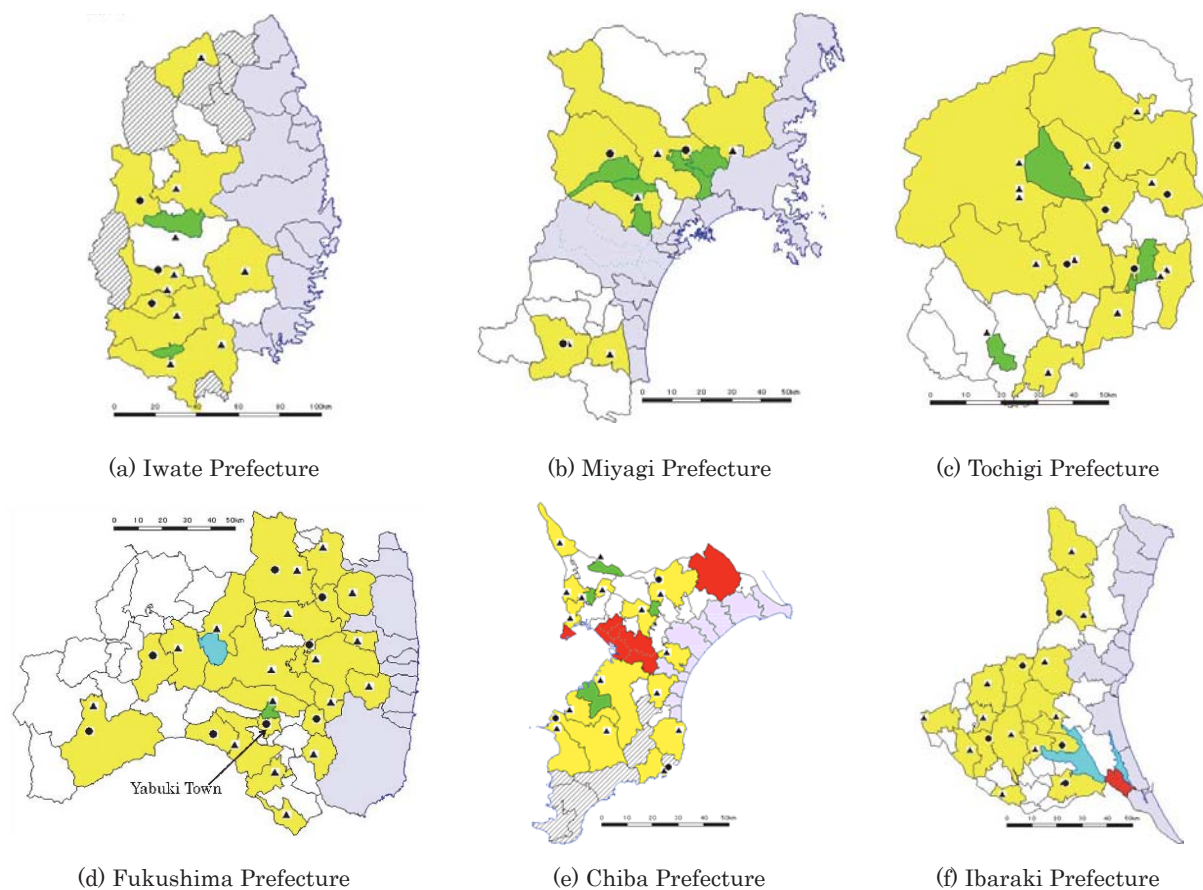


**Fig. 1** Stricken districts in the six prefectures studied in this paper. The districts colored yellow are our target areas; the gray districts mainly damaged by tsunami are excluded; the red districts affected by liquefaction are also excluded; the green districts are included as they are close to a strong-motion station; the blue areas are lakes; the shadowed districts with slashes are those lacking damage statistics; the marks ▲ and ● denote the positions of K-NET stations and KiK-net stations, respectively. This figure is plotted by the software, KenMap (2011).

instrumental foundation might cause extremely large motion, just as noted by Motosaka et al. (2011). On the other hand, those stations that are installed on rock and far from densely building-concentrated sites are also excluded regarding the representativeness of ground motions.

### 3. RELATIONSHIP BETWEEN BUILDING DAMAGE RATIOS AND GROUND MOTION CHARACTERISTICS

#### 3.1 Definitions of Three Kinds of Building Damage Ratios

The building damage ratios are composed of the following three indicators: total collapse ratio (TCR), collapse ratio (CR), and damage ratio (DR). Each of them is defined as the ratio of damaged buildings to total buildings in stricken districts. Detailed definitions are given as follows.

$$TCR = A/D \times 100\%, \quad (1)$$

$$CR = (A+B)/D \times 100\%, \quad (2)$$

$$DR = (A+B+C)/D \times 100\%, \quad (3)$$

Here, A, B, and C are the numbers of totally collapsed, half-collapsed, and partially damaged buildings in a district, respectively. D is the total number of buildings regardless of damage and non-damage in a district. In this paper, the damage data are obtained from the FDMA which publishes the damage data by the number of buildings. Therefore, denominator-D in Eq. (1) to Eq. (3) should also be the total number of buildings that can be obtained from the Statistics Bureau and Director-General for Policy Planning of Japan. However, the total numbers of buildings in some small districts cannot be obtained from the Statistics Bureau, but the total numbers of households in such districts can be easily found from the homepages of local governments and are taken as the total numbers of buildings. Fig. 2 shows the relationship between the total numbers of buildings and the total numbers of households in the stricken districts where both sets of data are available. It can be seen that the total number of households has a good correlation with the total number of buildings for each district, and the former is almost the same as the latter. This indicates that the total numbers of buildings can be replaced with the total numbers of households in those small districts in which the total number of households is fewer than

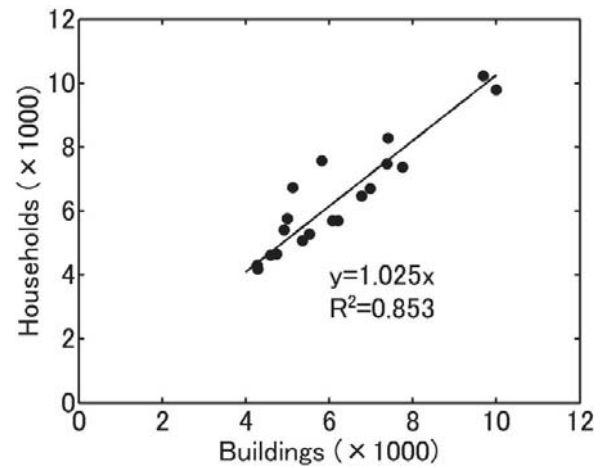


Fig. 2 Relationship between the number of buildings and the number of households.

10,000.

#### 3.2 Representativeness of Ground Motions in Stricken Districts

As the administrative unit of a stricken district is city, town, or village (*shi, cho, or mura* in Japanese), it might be reasonable to use the median ground motions in the entire district rather than the ground motions observed at the strong-motion stations. In Japan, the amplification factor for peak ground velocity (PGV) at a given site can be obtained from the J-SHIS website operated by the National Research Institute for Earth Science and Disaster Prevention (NIED, 2012). This suggests that the peak ground velocity on engineering bedrock,  $PGV_b$ , where the S-wave velocity is 400 m/s~600 m/s (NIED, 2009), can be obtained from the peak ground velocity on the ground surface,  $PGV_s$ , by dividing this factor at a given site. For an administrative unit,  $PGV_b$  can be assumed to be the same. Then, the median PGV on the ground surface for the entire district can be calculated mechanically from the  $PGV_b$  by multiplying the median amplification factor, as is expressed in the following equation.

$$PGV_m = PGV_b \times AVR_m = \frac{PGV_o}{AVR_o} \times AVR_m, \quad (4)$$

Here, AVR is the amplification factor, the subscript “m” is the median value for the entire district, and the subscript “o” is the observed value obtained from strong-motion data. Take Date City for example. Fig. 3 shows the distribution of amplification factors in Date City, Fukushima Prefecture. It can be seen

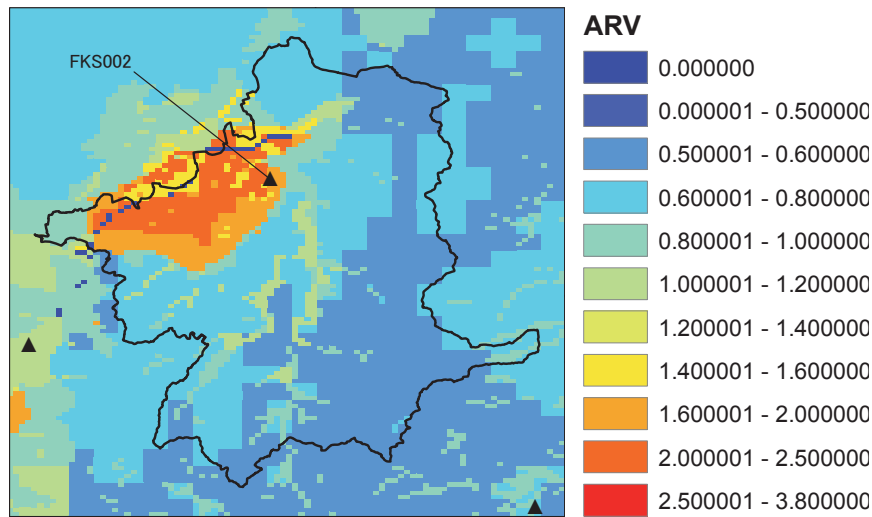


**Fig. 3** Distribution of amplification factors in Date City. The triangle denotes the strong-motion station (FKS002). The median amplification factor of Date City is 0.669, while the amplification factor at FKS002 is 1.997.

that there are warm-colored areas with large amplification factors in the northwest part of Date City. The strong-motion station, FKS002, indicated by a solid triangle, is situated just in this area. This suggests that the representative ground motions in Date City might be overestimated if the observed PGV at FKS002 is used. By finding the median amplification factor,  $AVR_m$ , of this city and the amplification factor,  $AVR_o$ , at FKS002, the median PGV can be obtained from the observed PGV at FKS002 by multiplying the ratio of  $AVR_m$  to  $AVR_o$ . Here,  $AVR_m/AVR_o$  is 0.669/1.997. That is, the representative PGV in Date City is about one-third of the observed PGV at FKS002. All the ground motions in the stricken districts should be revised as the median ground motions in the same way. However, it is advisable to use the median amplification factor only at sites where buildings are distributed. Unfortunately, this seems impossible as the exact distribution of buildings within a district is unknown. Generally, many buildings are concentrated in basins, or the warm-colored areas, with high amplification, and there are few buildings in hills, or the cold colored areas, with low amplification. Therefore, the representative ground motions for an entire district might be underestimated if they are revised in the way mentioned above. Eventually, the observed ground motions are assumed to be representative for an entire stricken district, as long as the strong-motion stations are not located on the rock. In Chapter 4, the effect of velocity structures on ground motions will be dis-

cussed in detail so as to understand ground motions at damaged sites.

### 3.3 Fragility Curves

Fragility curves are constructed to examine the relationships between three kinds of building damage ratios as well as the ground motion characteristics, which are peak ground acceleration (PGA), peak ground velocity (PGV), Japan Meteorological Agency instrumental seismic intensity ( $I_{JMA}$ ), and spectral intensity (SI). The cumulative probability of building damage,  $P(x)$ , is assumed to be the normal cumulative distribution function.

$$P(x) = \Phi((x - \lambda) / \zeta), \quad (5)$$

Here,  $\Phi$  is the standard normal cumulative distribution function.  $x$  is a variable with respect to ground motion indices, such as  $I_{JMA}$ , natural logarithm of PGA, natural logarithm of PGV, or natural logarithm of SI.  $\lambda$  and  $\zeta$  are the mean and standard deviation of  $x$ , and are determined by geometric mean regression with a normal probability plot. SI is defined as the integration of the velocity response spectrum with a damping coefficient of 0.20 averaged over a period of 0.1 s~2.5 s, as is shown in Eq. (6).  $I_{JMA}$  is calculated based on the manual issued by the Japan Meteorological Agency (1996). In addition, PGA, PGV, and SI are adopted to be the larger value between the NS and EW components.

$$SI = \frac{1}{2.5 - 0.1} \int_{0.1}^{2.5} SV(T) dT, \quad (6)$$

Here,  $SV$  is the velocity response spectrum with damping coefficient  $h=0.20$ .

Fig. 4 shows the fragility curves between three kinds of building damage ratios, i.e., TCR, CR, and DR, as well as the ground motion indices, i.e., PGA, PGV,  $I_{JMA}$ , and SI. The coefficients of  $\lambda$  and  $\zeta$ , and the determination coefficient  $R^2$  used to assess the goodness of fit, are given in Table 1. It can be seen that standard deviation  $\zeta$  between the DR and any one of the ground motion indices is the smallest, and that corresponding determination coefficient  $R^2$  is the largest among the three kinds of building damage ratios. This suggests that the correlation of ground motion indices with the DR is the best. Therefore, the relationship between the DR and the ground motion indices should be emphasized in the following analysis. From the values of  $R^2$ , it is implied that the correlation between the DR and  $I_{JMA}$  or SI is better than that be-

tween the DR and the PGA or PGV. From the values of  $\zeta$ , it can be seen that the variability between the DR and PGA is the largest. Combined with the above two coefficients, it can be seen that the correlation of the DR with the ground motion indices is approximately the same as one another, except with the PGA. However, variability generally arises between the DR and each of the four ground motion indices. One of the reasons for this is that the damage data are not classified by the building construction date and structural type in each stricken district. The different constitutive proportions of the building construction date or structural type in each stricken district can contribute to this variability. Furthermore, the damage data in some districts may include the numbers of damaged buildings not directly caused by ground shaking, such as landslide. However, the variability caused by these factors cannot be resolved until detailed damage data are obtained. Another reason may be that the ground motions at the strong-motion station are not appropriate for representing the ground motions for an entire

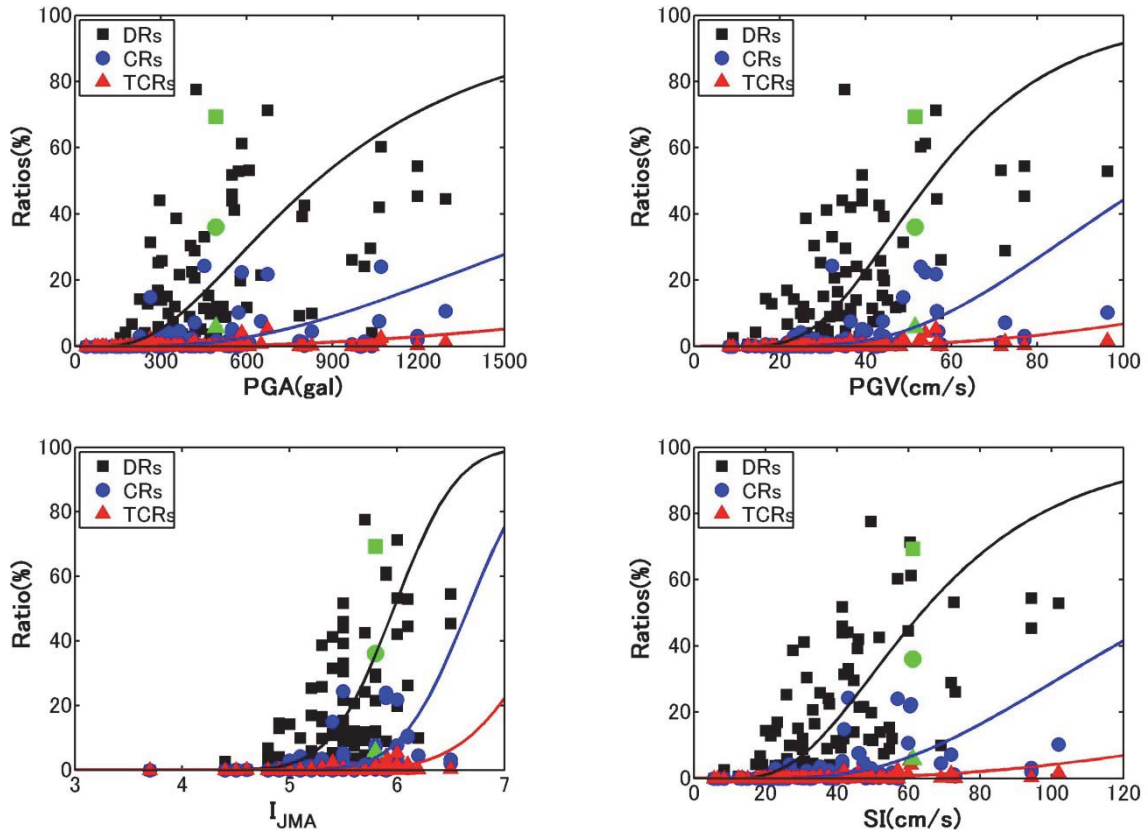


**Fig. 4** Fragility curves of the three kinds of building damage ratios versus PGA, PGV,  $I_{JMA}$  and SI. The green marks correspond to three kinds of building damage ratios in Yabuki Town, which will be discussed in Chapter 4.

**Table 1** Coefficients of the fragility curves.

Rank	PGA (gal)			PGV (cm/s)			I <sub>JMA</sub>			SI (cm/s)		
	$\lambda$	$\zeta$	R <sup>2</sup>	$\lambda$	$\zeta$	R <sup>2</sup>	$\lambda$	$\zeta$	R <sup>2</sup>	$\lambda$	$\zeta$	R <sup>2</sup>
TCR	8.680	0.843	0.146	5.613	0.674	0.352	7.499	0.651	0.281	5.869	0.728	0.292
CR	7.718	0.686	0.269	4.673	0.465	0.359	6.665	0.490	0.381	4.901	0.529	0.391
DR	6.738	0.638	0.478	4.009	0.432	0.420	5.971	0.464	0.543	4.153	0.502	0.509

stricken district. For example, if the strong-motion station is far away from the damaged sites, the ground motions for the entire district might be underestimated. The problem can be solved by the proposition introduced in Chapter 4. Additionally, the variability between the DR and PGA is larger than that between the DR and any of other three ground motion indices, which agrees with the conclusion of Midorikawa et al. (2011). This can be attributed to the sensitivity of PGA to the short-period characteristics of ground motions. Fig. 5 shows the damage data categorized by predominant period determined from the velocity response spectra. It can be seen that damage data of a short period of less than 0.4 s are mostly distributed beneath the fragility curve, i.e., large PGA with a short period of less than 0.4 s will not cause much damage to buildings. In contrast, the PGV seems to be insensitive to short periods of less than 0.4 s. Besides, both the PGA and PGV are not sensitive to longer periods of over 2.0 s which will not cause much damage to buildings, either. This suggests that PGA is not a good ground motion index for constructing a fragility curve.

### 3.4 Comparison of the 2011 Tohoku Earthquake with the Kobe Earthquake

Fig. 6 compares the 2011 Tohoku Earthquake with the Kobe Earthquake regarding four relationships: between DR and PGA, between DR and PGV, between DR and I<sub>JMA</sub>, and between DR and SI. It can be seen that the DR in the 2011 Tohoku Earthquake reaches almost the same level as that in the Kobe Earthquake in terms of I<sub>JMA</sub>,  $PGA \leq 800$  gal,  $PGV \leq 100$  cm/s, and  $SI \leq 100$  cm/s. Fig. 7 compares the 2011 Tohoku Earthquake with the Kobe Earthquake regarding the relationships between TCR and PGA, and between TCR and PGV. It can be seen that the TCRs for  $PGA \leq 800$  gal and  $PGV \leq 100$  cm/s during the 2011 Tohoku Earthquake are smaller than those during the Kobe Earthquake. This can be attributed to the different units used for the stricken districts. That is, the unit of stricken districts is “street” for the Kobe Earthquake, while the unit of stricken districts is “city,” “town,” or “village,” which are units much larger than “street,” for the 2011 Earthquake. As the number of totally collapsed buildings are very limited, the TCR calculated in a large district is naturally smaller than that calculated in a small district. It can also be seen that the TCRs for  $PGA > 800$  gal are close to zero. This might be caused by the

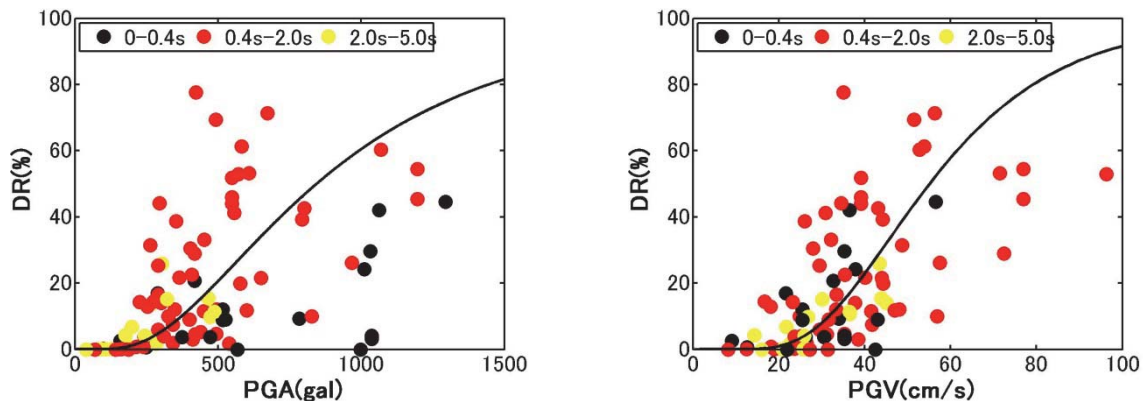


**Fig. 5** Classification of the damage data in the stricken districts by the predominant periods of velocity response spectra.

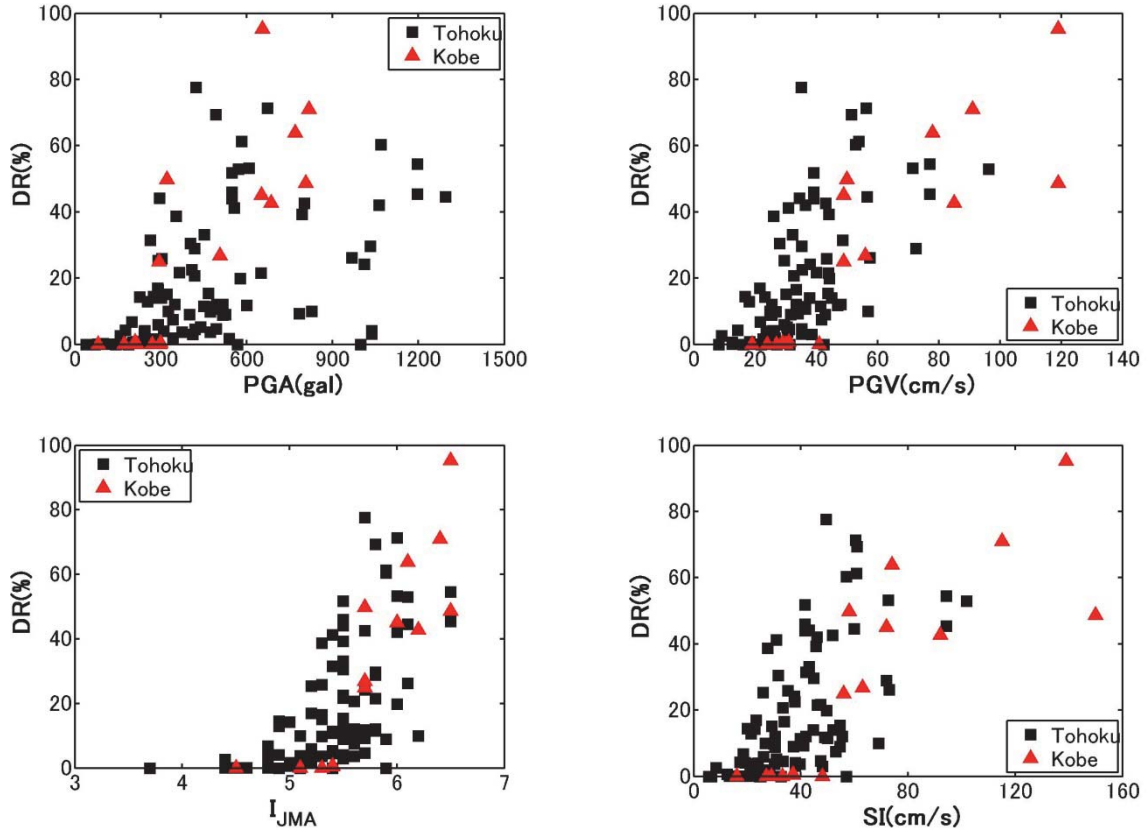


**Fig. 6** Comparison of damage data for DR between the Tohoku Earthquake and Kobe Earthquake. The damage data in the 17 stricken districts in the Kobe Earthquake are obtained from the paper of Yamaguchi and Yamazaki (1999).

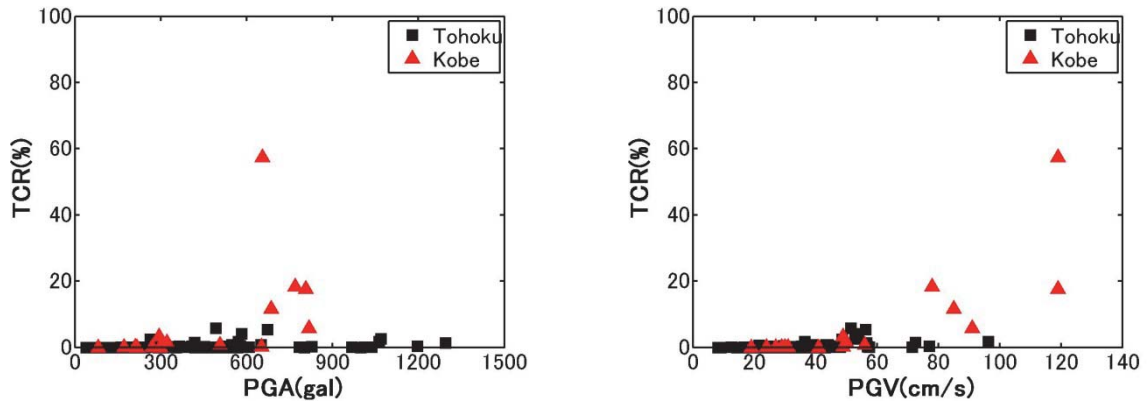


**Fig. 7** Comparison of damage data for CR between the 2011 Tohoku Earthquake and Kobe Earthquake.

short-period characteristics of ground motions.

Fig. 8 shows the relationship between PGA, PGV, and DR. PGA and PGV are the maximum values of vector summation in three components in this figure. The straight solid line is plotted according to the different equivalent predominant period,  $T_{eq}$ , which is defined as  $T_{eq}=2\pi PGV/PGA$ . DR is divided into

four levels, i.e.,  $0\% \leq DR < 20\%$ ,  $20\% \leq DR < 40\%$ ,  $40\% \leq DR < 60\%$ , and  $60\% \leq DR \leq 80\%$ . It can be seen that the equivalent predominant period of most damage data ranges from 0.2 s to 1.0 s. In particular, the equivalent predominant period of the damage data for  $60\% \leq DR \leq 80\%$  is around 0.5 s, and the corresponding  $PGA \geq 450$  gal, as well as  $PGV \geq 35$  cm/

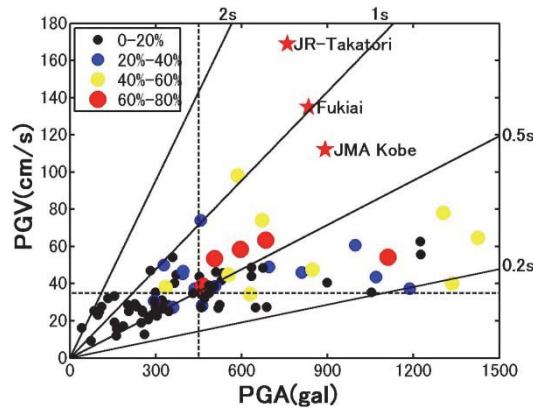


**Fig. 8** Relationship between PGA, PGV and DR. The solid lines show the equivalent predominant periods ( $T_{eq}=2\pi PGV/PGA$ ;  $T_{eq}=0.2s, 0.5s, 1.0s, 2.0s$ ). The dotted lines are the thresholds of PGA and PGV for  $60\% \leq DRs \leq 80\%$ . Note that PGA and PGV are the maximum values of vector summation in three components. The PGA and PGV in the stricken districts of Kobe Earthquake are obtained from the paper of Kawase (1998).

s. Fig. 8 also shows the stricken districts in the Kobe Earthquake, i.e., JR-Takatori (DR=95.3%), JMA Kobe (DR=71.0%), and Fukiai (DR=48.7%). It can be seen that the equivalent predominant period during the 2011 Earthquake is shorter than that during the Kobe Earthquake. On the other hand, the largest PGA among the stricken districts used in this paper during the 2011 Tohoku Earthquake is larger than that during the Kobe Earthquake, yet the largest PGV among the stricken districts used in this paper during the 2011 Tohoku Earthquake is smaller than that during the Kobe Earthquake.

#### 4. ESTIMATION OF GROUND MOTIONS AT DAMAGED SITES

From the fragility curves, we found there are some sites where the level of ground motion characteristics does not correspond to the DRs, such as Yabuki Town. The level of ground motions in Yabuki

Town shown with the green marks in Fig. 4 is not very high, but the DR is rather large. Muraibo et al. (2011) conducted a building damage survey in Yabuki Town and published the numbers of damaged buildings in the villages within Yabuki Town on November, 2011, as shown in Table 2. Obviously, the DR at Ippongi Village where the strong-motion station FKSH11 is installed is the smallest among all the villages in Yabuki Town. Therefore, the ground motions at FKSH11 are not appropriate for representing the ground motions for entire Yabuki Town. It is desirable to construct fragility curves based on a smaller administrative unit, such as “street”. Therefore, it is important to find a way to estimate ground motions at sites where ground motion records during the main-shock were not obtained. In this section, a method of estimating ground motions is proposed. To construct fragility curves with greater accuracy, the ground motions at damaged sites should be estimated based on the information on velocity structures under the sites.

**Table 2** Numbers of damaged buildings in each village of Yabuki Town.

Name	No damage	Slight damage	Minor damage	Moderate damage	Heavy damage	Collapse	Unknown	DR (%)
Tatesaza	22	16	12	0	4	0	0	59.3
Ohmachi	40	38	20	3	3	0	1	61.0
Motomachi	101	73	27	16	14	2	9	54.5
Nakamachi	100	142	58	56	40	4	17	71.9
Shimachi	96	86	17	6	6	3	1	54.9
Yamatouchi	21	15	16	4	14	1	0	70.4
Ippongi	37	32	1	0	0	0	0	47.1

As a case study, the ground motions at Yamatouchi in Yabuki Town are estimated.

#### 4.1 Methodology for Estimating Ground Motions at Damaged Sites

In general, ground motion spectrum  $O_i(f)$  on the surface at the  $i_{th}$  site can be expressed as the product of source spectrum  $S_i(f)$ , path spectrum  $P_i(f)$ , and transfer function  $G_i(f)$ , as is expressed in Eq.(7). Because input motion spectrum  $B_i(f)$  can be defined as the product of source spectrum  $S_i(f)$  and path spectrum  $P_i(f)$ , the ground motion spectrum  $O_i(f)$  is also expressed by Eq.(8).

$$O_i(f) = S_i(f) \cdot P_i(f) \cdot G_i(f), \quad (7)$$

$$O_i(f) = B_i(f) \cdot G_i(f), \quad (8)$$

Transfer function  $G_i(f)$  is defined as the surface response to input motion from a common basement. Here, the common basement suggests that the velocity structures under the basement are almost the same at the sites. Following Eq. (8), the input motion spectrum can be calculated from the ground motion spectrum divided by the transfer function, as is expressed in Eq. (9).

$$B_i(f) = O_i(f) / G_i(f), \quad (9)$$

Supposing that the strong-motion station ( $i=0$ ) and the surrounding damaged site ( $i=1$ ) are not far from each other compared with the distance between the site and the source, e.g., less than 10 km, the input motion can be assumed to be the same, i.e.,  $B_0(f) = B_1(f)$ , as long as a common basement exists. Then, ground motion spectrum  $E_1(f)$  at the damaged site can be expressed as a product of input motion spectrum  $B_0(f)$  at the strong-motion station and transfer function  $G_1(f)$  at the damaged site.

$$E_1(f) = B_0(f) \cdot G_1(f) = O_0(f) / G_0(f) \cdot G_1(f), \quad (10)$$

Because ground motion spectrum  $O_0(f)$  is known at any strong-motion station, the ground motion spectrum  $E_1(f)$  at the damaged site close to the strong-motion station can be obtained if the transfer functions both at the strong-motion station and at the damaged site are estimated.

As the transfer functions depend on the underground velocity structures, it is essential to obtain reliable S- and P-wave velocity structures. For a KiK-net station, the underground velocity structures

between the surface and the borehole sensors can be obtained either directly from the PS-logging data or indirectly from the spectral ratios between the surface and the borehole sensors. For other sites where there are neither strong-motion data nor PS-logging data, velocity structures can be identified from the microtremor H/V spectral ratio, such as conducted by Arai and Tokimatsu (2004). They estimated the S-wave velocity structures by assuming that microtremors are dominantly composed of surface waves. On the other hand, Sánchez-Sesma et al. (2011) noted that the microtremor H/V spectral ratio can be expressed as the square root of the ratio of the corresponding imaginary parts of Green's tensor components in three dimensions by assuming that the seismic field of microtremors is diffusive. They succeeded in interpreting the microtremor H/V spectral ratio recorded at a site close to Mexico City with this theory. Kawase et al. (2011) applied this theory to the analysis of earthquake ground motions and found that the imaginary part of Green's function for plane waves at the free surface is proportional to the square of the absolute value of the corresponding transfer function. They further noted that the H/V spectral ratio of earthquake ground motions can be theoretically calculated as the amplitude ratio between transfer functions for S-wave and P-wave based on diffuse-field theory, both calculated at the strong-motion station with a coefficient depending on the bedrock. They also suggested that the earthquake H/V spectral ratio can be used to identify the velocity structures. Following Kawase's viewpoint, we attempt to examine whether the H/V spectral ratio of microtremors can also be used to identify the velocity structures, after confirming the consistency of H/V spectral ratios between microtremors and earthquake ground motions.

Before applying our method, the effectiveness of Kawase's proposition is verified by the following procedures.

- (a) Identifying the S- and P-wave velocity structures between the surface and borehole sensors from the spectral ratios of small earthquakes ( $M \leq 5.0$ ;  $PGA < 100$  gal) at KiK-net stations.
- (b) Confirming that the H/V spectral ratio of earthquake ground motions is consistent with the theoretical H/V spectral ratio calculated with identified velocity structures and veloci-

ty structures under a common basement. This in turn suggests that the underground velocity structures can be identified from the H/V spectral ratio of earthquake ground motions, which agrees with Kawase's proposition. At the same time, the transfer function between the surface and basement can be obtained at strong-motion stations.

Then, the consistency of H/V spectral ratios between earthquake ground motions and microtremors is examined at the strong-motion stations. If they are almost identical to each other, the underground velocity structures at damaged sites close to strong-motion stations can be identified from the H/V spectral ratios of microtremors by assuming that the H/V spectral ratios of microtremors would also be consistent with those of earthquake ground motions at damaged sites.

After that, the transfer function at damaged sites can be obtained with identified velocity structures and the velocity structures under a common basement. Finally, the ground motions can be estimated through Eq. (10) in the case of linear behavior. Nonlinear behavior of soil will be discussed later.

## 4.2 Case study at a Damaged Site

### 4.2.1 Verification of Kawase's proposition at KiK-net stations

As there are two seismographs both on the surface and the bottom of the borehole at KiK-net stations, the underground velocity structures between surface and borehole sensors can be identified from the observed spectral ratios between surface and borehole sensors. To avoid the nonlinear effect on ground motions during a mainshock, small earthquakes should be considered in the calculation of spectral ratios.

At FKSH11, the KiK-net station in Yabuki Town, ground motions from nine small earthquakes are selected for calculating the spectral ratios listed in Table 3. The S-wave parts with a duration of 20.48 s measured from the onset time (the duration of all the waveforms is 120 s) are analyzed. The initial velocity structure model is obtained from the PS-logging data of the National Research Institute for Earthquake Science and Disaster Prevention (NIED). Quality factor  $Q_s$  is taken as  $Q_0 \cdot f^n$ .  $Q_p$  is assumed to be simply  $Q_s/2$  (Yoshida and Kobayashi, 2002). Initial  $Q_0$  is taken as one-twentieth of the S-wave logging velocity. First, the S-wave velocity structures including the S-wave velocity,  $Q_0$ , and exponent  $n$  in each layer are identified with the simulated annealing algorithm (e.g., Ingber, 1989; Saguchi, et al., 2009). Then, the P-wave velocity in each layer is identified assuming that  $Q_p = Q_s/2$ . After that, the velocity structures under a common basement are assumed, as there is not sufficient information about them, but they are indispensable for interpreting the H/V spectral ratio on the surface.

Table 4 lists the initial velocity structures, i.e., the PS-logging data, between the surface and the borehole sensors ( $-115.2$  m) and the identified velocity structures, as well as the velocity structures under a common basement at FKSH11. Fig. 9 shows the observed spectral ratios between surface and borehole sensors for small earthquakes and the theoretical spectral ratios calculated with identified velocity structures for horizontal components and those for vertical components, respectively. By matching the observed horizontal and vertical spectral ratios with the theoretical ratios, the optimum S- and P-wave velocity structures are obtained, respectively, as shown in Fig. 10. It can be seen from Fig. 9 (a) that the peak value at 0.7 s of the theoretical spectral ratio for the S-

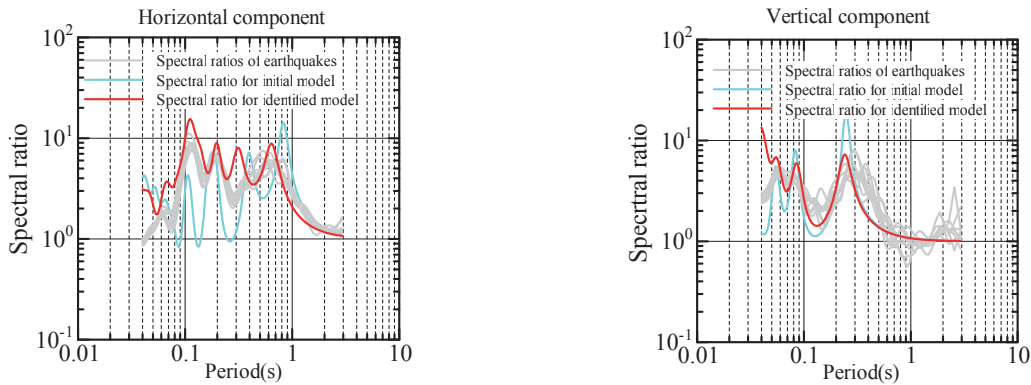
**Table 3** Source information about small earthquakes used in the analysis for FKSH11.

Date (yy/mm/dd)	Origin time	Latitude (N)	Longitude (E)	Depth (km)	M	PGA (gal)
11/10/26	2:08:52	36.96	141.15	30	5.0	17.8
11/08/22	21:21:23	37.18	141.22	31	4.1	12.1
11/05/17	0:53:33	37.38	141.30	35	4.6	13.4
11/05/01	11:48:46	37.42	141.21	29	4.6	13.1
11/04/30	14:46:59	37.34	141.29	33	4.5	9.5
11/04/18	0:47:29	37.00	141.28	29	4.8	15.6
11/04/11	13:51:45	37.47	141.32	29	5.0	12.2
11/04/01	2:21:36	36.96	141.22	34	4.4	6.8
11/03/21	4:54:20	37.30	141.20	30	4.7	11.2

**Table 4** Initial and identified velocity structures at FKSH11.

Density (g/cm <sup>3</sup> )	V <sub>p0</sub> (m/s)*	V <sub>s0</sub> (m/s)*	V <sub>p</sub> (m/s)	V <sub>s</sub> (m/s)	Thickness (m)	Q <sub>0</sub>	n
1.7	200	110	109	33	1	6.3	0.41
1.9	1600	250	1168	153	3	22.4	1
1.9	1600	250	1054	191	7.5	22.5	1
1.9	1600	250	1255	192	7.5	4.0	0.21
1.9	1600	250	1503	240	7.5	10.24	0.8
1.9	1600	250	1498	300	7.5	22.48	1
2.1	2200	1200	1777	847	11	35.62	0.99
2.1	2200	1200	2122	1059	11	42.0	1
2.0	1700	490	1500	851	15	5.0	0.47
2.0	1700	490	1532	882	15	19.0	0.03
2.2	1900	700	2410	1208	14.6	47.0	0.71
2.2	1900	700	2481	1260	14.6	47.0	0.71
2.3	-	-	3120	1800	100	50.0	1
2.4	-	-	4330	2500	100	50.0	1
2.5	-	-	5900	3400	∞	50.0	1

\* The PS-logging data obtained from the NIED are used as the initial model.



(a) Spectral ratios in the horizontal component

(b) Spectral ratios in the vertical components

**Fig. 9** Observed spectral ratios (gray) between surface and borehole sensors for small earthquakes and theoretical spectral ratios calculated with the initial (blue) and identified (red) S- and P-wave velocity structures.

wave and the curve shape are similar to the observed spectral ratios for small earthquakes in the horizontal component. It can also be seen from Fig. 9 (b) that the theoretical spectral ratio for the P-wave is in good agreement with the observed ratios in the vertical component.

Fig. 11 shows four different H/V spectral ratios, the observed ones for S-wave motions and coda motions, and the theoretical ones for S- and P-waves and Rayleigh waves. It can be seen that the theoretical H/V spectral ratio for S- and P-waves using the identified S- and P-wave velocity structures and the common basement velocity structures matches well with the average H/V spectral ratios for the observed S-

wave motions and coda motions (duration of 20.48 s) from small earthquakes. It can be seen that they fit well with one another, especially for the peak value at about 0.12 s and 0.70 s. This in turn suggests that the underground velocity structures can be obtained from the H/V spectral ratio of small earthquakes, which agrees with Kawase’s proposition. In addition, the predominant periods of the ellipticity of the Rayleigh waves at about 0.12 s and 0.70 s are consistent with those of the theoretical H/V spectral ratio for the S- and P-wave. This indicates that the velocity structures between the surface and –115.2 m identified from the spectral ratios are valid and reliable.

Verification should be conducted at any one of

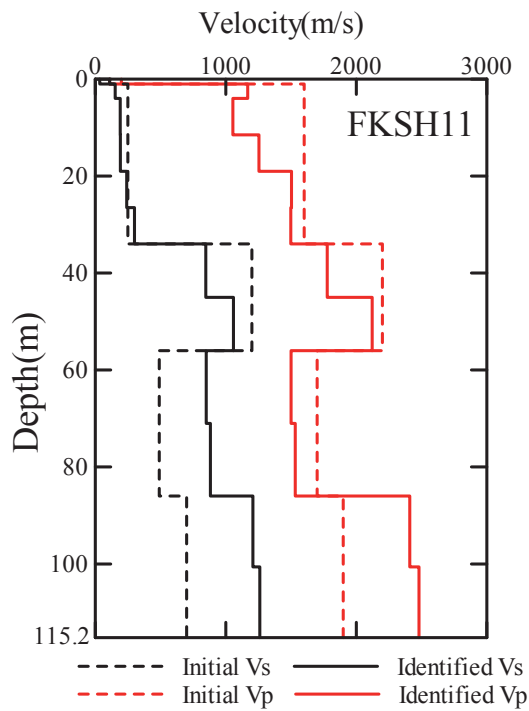


**Fig. 10** Profiles of initial (broken line) and identified (solid line) velocity structures between surface and borehole sensors ( $-115.2$  m) at FKSH11.

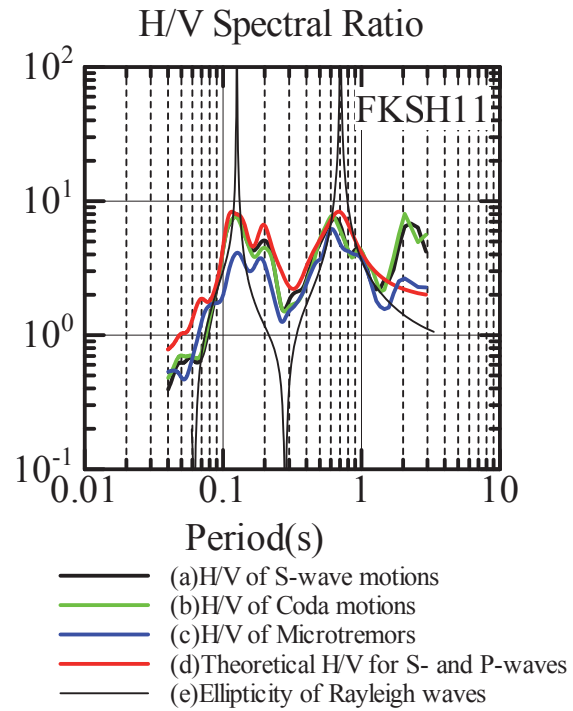


**Fig. 11** Comparison of the following four ratios: average H/V spectral ratios of S-wave motions (a) and coda motions (b) for small earthquakes, theoretical H/V spectral ratio (c) for S- and P-waves calculated with the identified S- and P-wave velocity structures at FKSH11, and the ellipticity of the Rayleigh waves (d).

the KiK-net stations in the same way. Fig. 12 gives another example at IBRH16 in Hitachiomiya City, Ibaraki Prefecture.

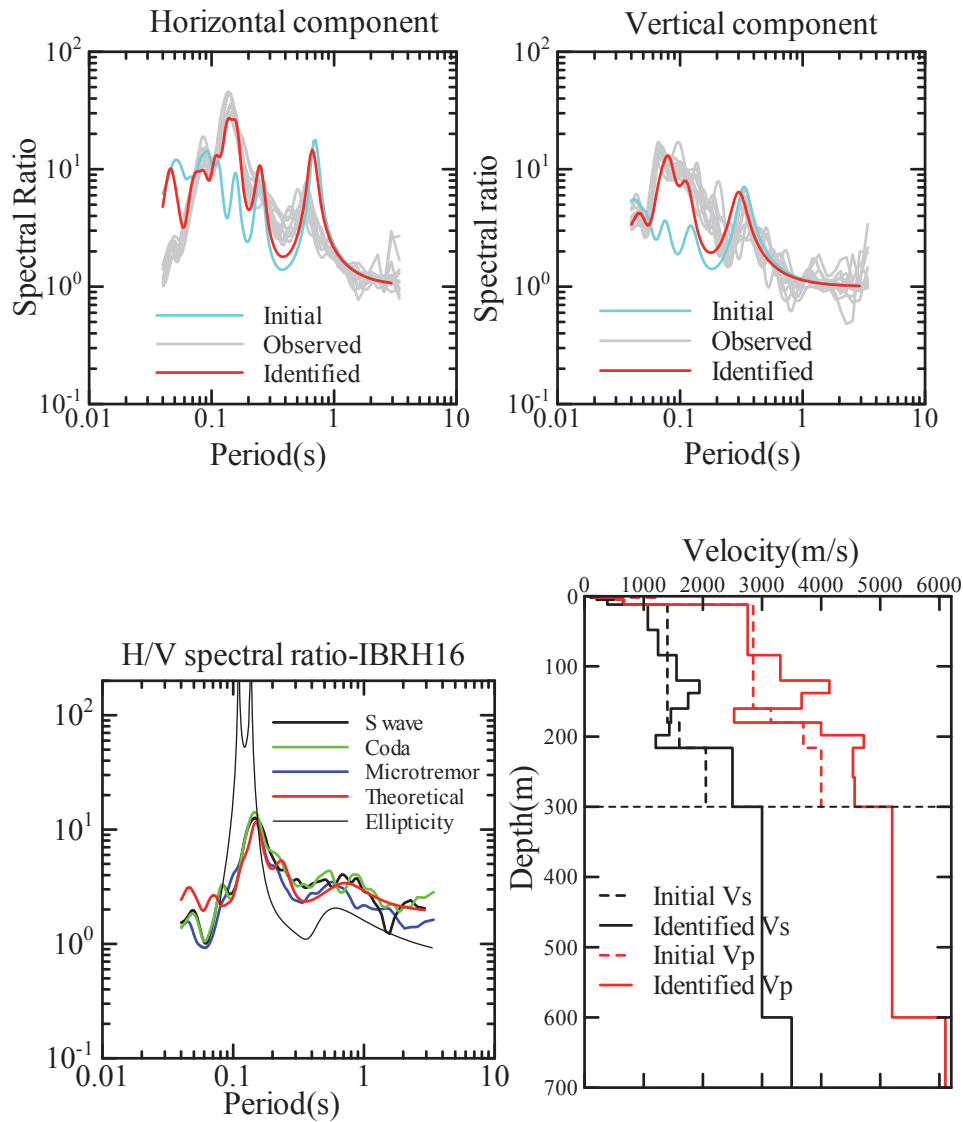
#### 4.2.2 Consistency of H/V Spectral Ratios between Earthquake Ground Motions and Microtremors

Fig.13 shows a comparison of the observed H/V spectral ratios between earthquake ground motions and microtremors. It can be seen that the H/V spectral ratio of microtremors is highly consistent with that of earthquake ground motions at FKSH11 of Yabuki Town and IBRH16 of Hitachiomiya City, not only the spectral shape but also the amplitude. At TCGH10 in Otahara City, it can be seen that the fundamental mode of H/V spectral ratios of microtremors and earthquake ground motions is almost the same, but that the amplitude is different, i.e., the amplitude of the H/V spectral ratio of microtremors is lower than that of earthquake ground motions. This may be caused by the small velocity contrast between the

surface layers and the deeper layers. Fig. 14 shows the velocity structures obtained from the PS-logging data, NIED. It can be seen that the velocity contrast is not very large, compared with the velocity structures at FKSH11 or IBRH16. At MYG013, Sendai City, neither the fundamental mode nor the amplitude of the H/V spectral ratio of microtremors is consistent with that of the H/V spectral ratio of earthquakes. The irregular underground velocity structures are considered to be one of the reasons, except the small velocity contrast in the surface layers. If the consistency of the H/V spectral ratios between earthquake ground motions and microtremors cannot be confirmed, how to apply the H/V spectral ratio of microtremors to the estimation of ground motions will be a subject of our future study.

#### 4.2.3 Identification of velocity structures and estimation of ground motions at the damaged site

Yamatouchi is one of the damaged sites in Ya-



**Fig. 12** Identification of velocity structures at IBRH16, Hitachiomiya City, Ibaraki Prefecture. The theoretical H/V ratio for S- and P-waves calculated with the identified velocity structures and the basement velocity structures agrees well with the observed H/V spectral ratios of both microtremors and earthquake ground motions. The consistency of the fundamental mode of the ellipticity of Rayleigh waves with those of theoretical H/V spectral ratios for S- and P-waves suggests that the identified velocity structures are valid.

buki Town. Fig. 15 is a snapshot trimmed from the Seamless Geological Map of Japan (2012). The distance between FKSH11 and Yamatouchi is about 3 km. The geologic time and rock type of the surface geology at both sites are almost the same. As the H/V spectral ratios of the microtremors and earthquake ground motions are consistent with each other at FKSH11, it is reasonable to assume that the consistency is invariable at Yamatouchi close to FKSH11 and that these two sites share a common basement. Then, the underground velocity structures at Yamatouchi in Yabuki Town can be identified from the

H/V spectral ratio of microtremors. The method of identifying the velocity structures at Yamatouchi is almost the same as that at FKSH11, but the target is replaced with the H/V spectral ratio of microtremors. The initial model at Yamatouchi is assumed to be the same as the identified one at FKSH11 except the first layer because the identified velocities of the first layer at FKSH11 are too slow. The initial model of the first layer at Yamatouchi is assumed to be the PS-logging data of FKSH11. Table 5 lists the initial and identified S- and P-wave velocity structures and those underlain by a common basement. The profile of the identified

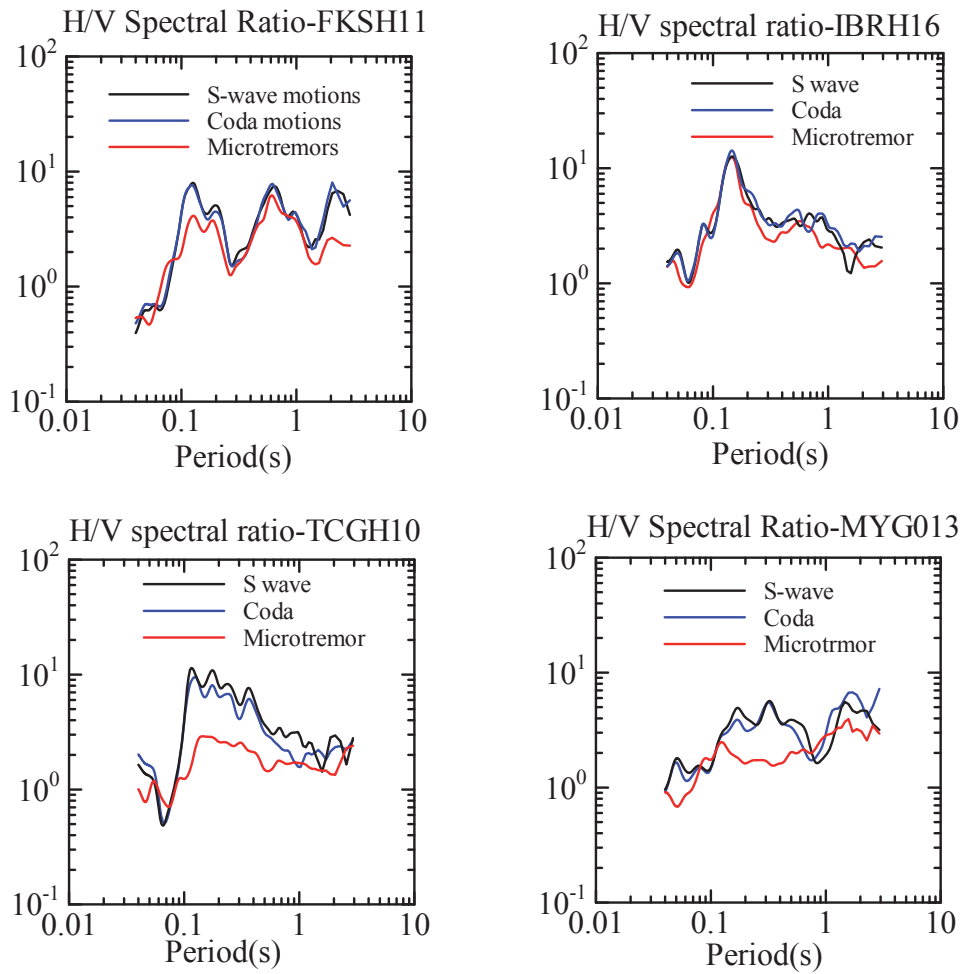


Fig. 13 Comparison of H/V spectral ratios between earthquake ground motions and microtremors.

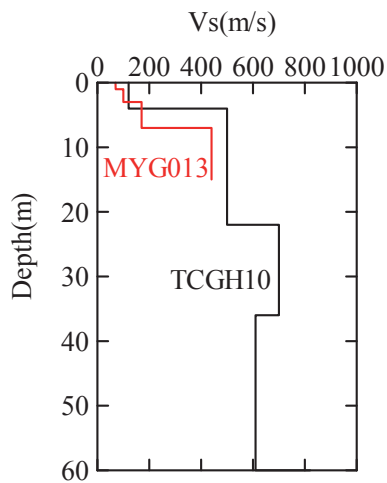


Fig. 14 Profiles of S-wave velocities at TCGH10 (black) and MYG013 (red) obtained from PS-logging data.

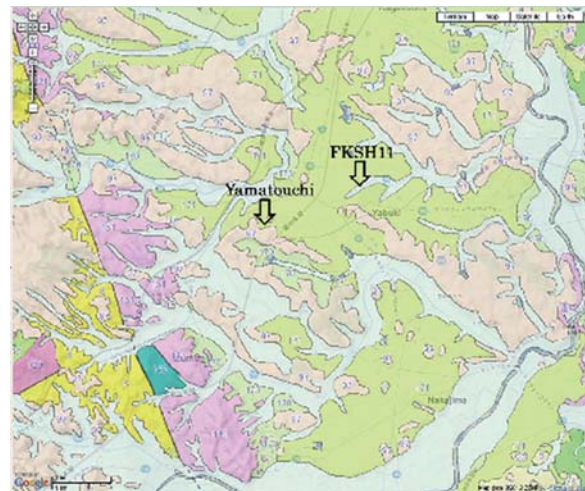


Fig. 15 Snapshot trimmed from the Seamless Geological Map of Japan. The geologic time is Late Pleistocene to Holocene, and the lithology is marine and non-marine sediments at FKSH11. The geologic time is Late Pleistocene, and the lithology is middle terrace at Yamatouchi.

**Table 5** Identified velocity structures at Yamatouchi.

Density (g/cm <sup>3</sup> )	Vp <sub>0</sub> (m/s)*	Vs <sub>0</sub> (m/s)*	Vp (m/s)	Vs (m/s)	Thickness (m)	Q <sub>0</sub>	n
1.7	200*	110*	434	139	1	7.9	0.96
1.9	1168	153	1382	159	3	6.4	0.33
1.9	1054	191	820	211	7.5	9.9	0.15
1.9	1255	192	2038	150	7.5	6.7	0.07
1.9	1503	240	2417	221	7.5	6.8	0.52
1.9	1498	300	946	198	7.5	6.4	0.00
2.1	1777	847	2692	1485	11	74.5	0.96
2.1	2122	1059	1868	1007	11	51.0	0.70
2.0	1500	851	2484	654	15	8.7	0.13
2.0	1532	882	2317	549	15	9.1	0.18
2.2	2410	1208	2779	576	14.6	16.3	0.26
2.2	2481	1260	2721	1099	14.6	85.3	0.37
2.3	3120	1800	3120	1800	100	50.0	0.50
2.4	4330	2500	4330	2500	100	50.0	0.50
2.5	5900	3400	5900	3400	∞	50.0	0.50

\* The initial model at Yamatouchi is assumed to be the same as the identified model of FKSH11 except the first layer (PS-logging data at FKSH11 are used)

velocity structures between the surface to -115.2 m is also shown in Fig. 16. Fig. 17 shows a comparison between the H/V spectral ratio of microtremors and

the theoretical H/V spectral ratio for S- and P-wave calculated with the underground velocity structures at Yamatouchi. The good fitting between the observed

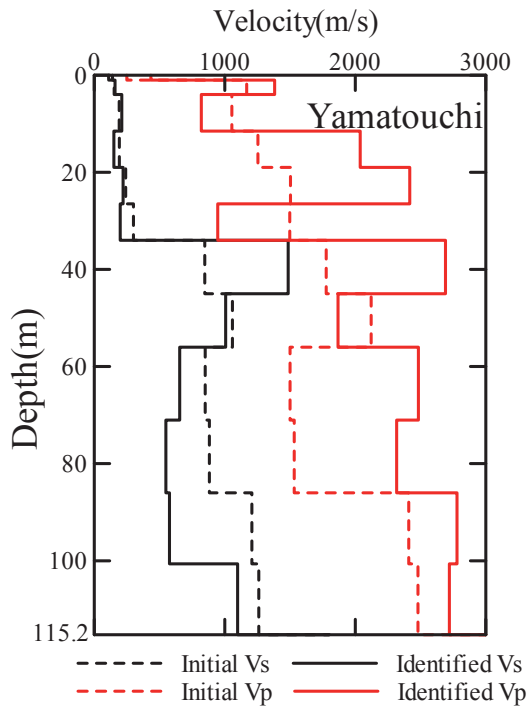


**Fig. 16** Profiles of initial (broken line) and identified (solid line) velocity structures between the surface and -115.2 m at Yamatouchi.

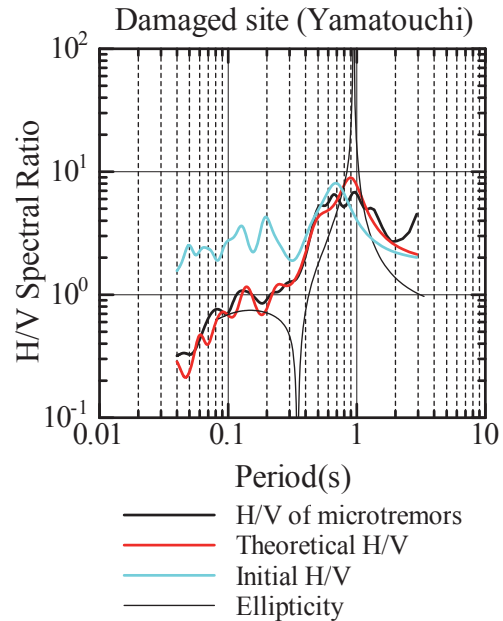


**Fig. 17** Comparison of the H/V spectral ratio of microtremors, the theoretical H/V spectral ratio calculated with identified velocity structures, and velocity structures underlain by a common basement at Yamatouchi, the theoretical H/V spectral ratio calculated with initial velocity structures, and the ellipticity of Rayleigh waves.

H/V spectral ratio and the theoretical H/V spectral ratio, especially the peak value at about 0.90 s and the spectral shape around the predominant period, suggests that the identified velocity structures are reliable at Yamatouchi. Fig. 17 also shows the ellipticity of the Rayleigh waves. It can be found that the fundamental mode of the ellipticity is highly consistent with that of other H/V spectral ratios. This indicates that the method of identifying velocity structures from the H/

V spectral ratio of microtremors is valid and reliable.

Based on the underground velocity structures at FKSH11 and Yamatouchi, the transfer functions can be obtained. Fig. 18 shows the transfer functions both at FKSH11 and Yamatouchi. It can be seen that the transfer function at FKSH11 is much larger than that at Yamatouchi in the short-period range, i.e., less than 0.3 s, but it is smaller at about 1.0 s. Then, ground motions at Yamatouchi are estimated from the transfer functions at FKSH11 and Yamatouchi and the ground motions at FKSH11. Fig. 19 compares the estimated velocity waveforms in three components at Yamatouchi with the observed velocity waveforms at FKSH11. Table 6 compares the estimated ground motion indices of Yamatouchi with those of FKSH11. It can be seen that the ground motion indices at Yamatouchi are larger than those at FKSH11, except the PGA, which may be caused by the smaller transfer function in the short-period range. Fig. 20 shows the pseudo-velocity response spectra (pSv) at Yamatouchi and FKSH11. It can be seen that Yamatouchi has a larger pSv of about 400 cm/s around the 1.0 s period than the pSv of about 200 cm/s at FKSH11. This can be explained by the larger transfer function at about 1.0 s for Yamatouchi. The larger ground motion indices except PGA and the larger pSv at Yamatouchi agree with the DR as high as 70%. Therefore, the proposition of identifying the velocity structures from the H/V spectral ratio of earthquake ground motions by Kawase et al.

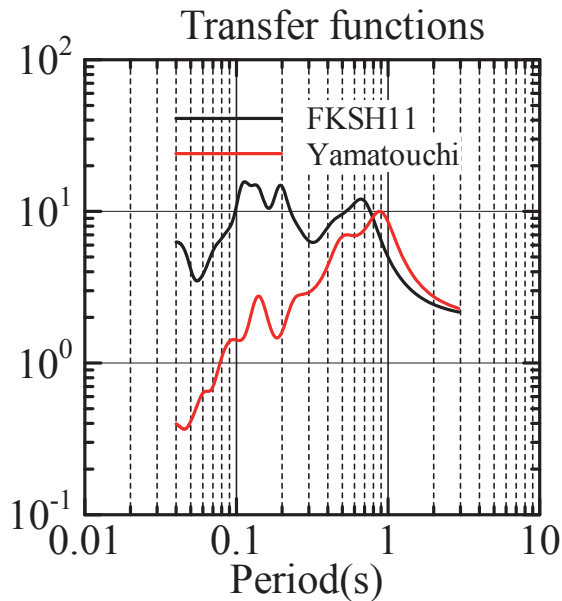


Fig. 18 Transfer functions between FKSH11(black) and Yamatouchi (red).

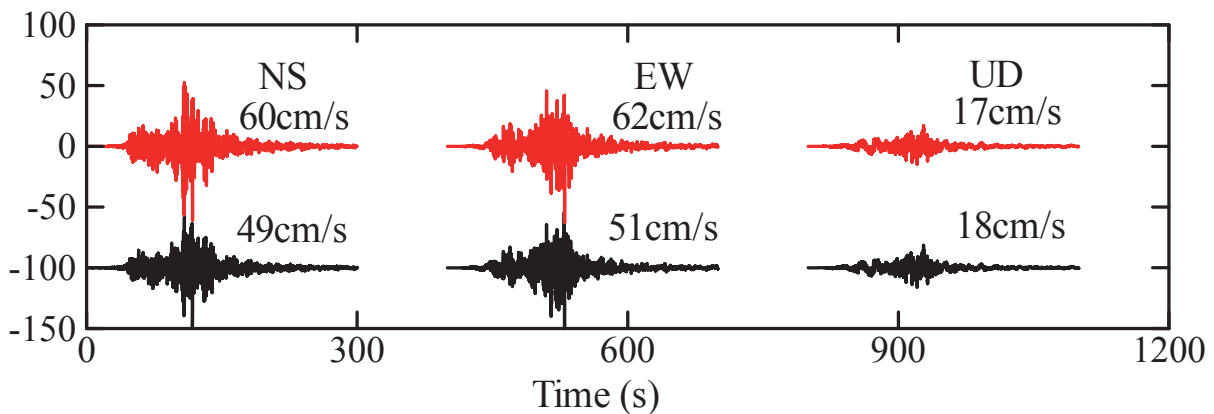


Fig. 19 Velocity waveforms at Yamatouchi (top) and FKSH11 (bottom).

Table 6 Ground motion indices at Yamatouchi and FKSH11.

	PGA (gal)	PGV (cm/s)	I <sub>JMA</sub>	SI (cm/s)
Yamatouchi	440	62	6.0	77
FKSH11	492	51	5.8	61

(2011) is proved to be applicable to microtremors. It can be applied to estimate the ground motions at damaged sites as long as the consistency of H/V spectral ratios between microtremors and earthquake ground motions is confirmed at strong-motion stations close to damaged sites.

### 5. DISCUSSION

Estimation of ground motions at damaged sites was performed on the basis of a linear assumption in this study, but nonlinear behavior was confirmed at many K-NET and KiK-net stations during the mainshock. Fig. 21 shows the H/V spectral ratios of the mainshock and small earthquakes at FKSH11 in Yabuki Town. It can be seen that the peak of the H/V spectral ratio shifts from about 0.12 s to 0.15 s during the mainshock, yet the peaks at 0.70 s and 1.0 s are invariable. This suggests that the shallow surface soil layers behave nonlinearly during the mainshock. However, the period of the ground motions that relates with building damage is usually around 1.0 s. Thus, the nonlinear behavior of surface soil will only affect ground motions in the short-period range, while this effect on ground motions might not be related to the building damage. Therefore, the estimated ground motions both at the basement of FKSH11 and on the surface of Yamatouchi are reasonable even if the non-

linear effect is not considered.

The objective of estimation of ground motions at damaged sites is to reduce the variability of the current fragility curves and to construct fragility curves with greater accuracy. In order to obtain fragility curves with greater accuracy, damage data and the corresponding estimated ground motions at damaged sites should be used. Unfortunately, the estimation of the ground motions is only conducted at one damaged site. More microtremor measurements and more estimation of the ground motions at damaged sites should be the focus of our work in the near future.

### 6. CONCLUSIONS

The fragility curves are investigated based on the relationships between the building damage ratios (i.e., TCR, CR and DR) and ground motion characteristics in the stricken districts in the East Tohoku and East Kanto region during the 2011 Tohoku Earthquake. Then the features of ground motions and damage ratios are compared with those of the Kobe Earthquake. Finally a method of estimating the ground motions was proposed using the velocity structures identified from the H/V spectral ratios of microtremors at the damaged sites. This method is expected to be used to construct fragility curves with greater accuracy. The following conclusions are obtained:

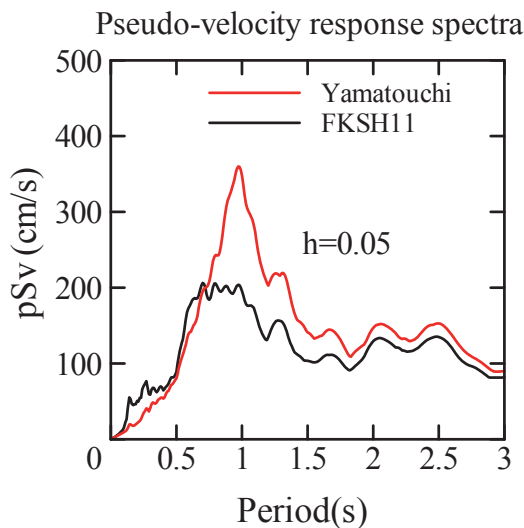


**Fig. 20** Pseudo-velocity response spectra (damping ratio  $h=0.05$ ) of the vector summation for the horizontal component at Yamatouchi and at FKSH11.

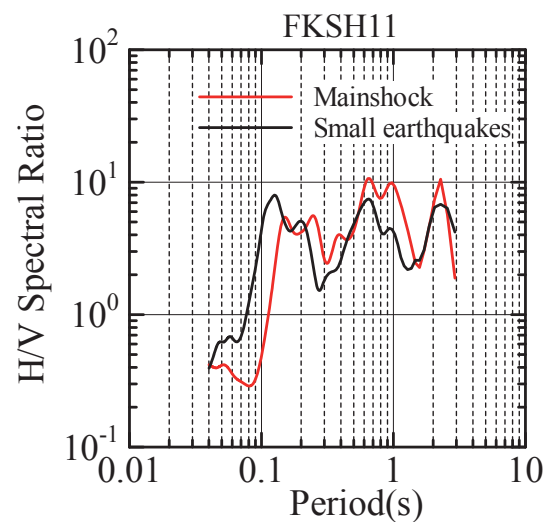


**Fig. 21** H/V spectral ratios of the mainshock and small earthquakes at FKSH11.

(1) DR relates better to the ground motion indices, i.e., PGA, PGV,  $I_{JMA}$ , and SI, than TCR or CR. The correlations for DR versus PGV, DR versus  $I_{JMA}$ , and DR versus SI are almost the same as one another. The relationship between DR and PGA has larger variability than the relationships between DR and PGV, between DR and  $I_{JMA}$ , and between DR and SI, because PGA is more sensitive to the predominant period. Even large PGA is not always related to high DR if the predominant period is shorter than 0.4 s.

(2) DR for the 2011 Tohoku Earthquake is almost the same as those for the Kobe Earthquake for the same level of ground motions in terms of  $I_{JMA}$ ,  $PGA \leq 800$  gal,  $PGV \leq 100$  cm/s, and  $SI \leq 100$  cm/s.

(3) DRs greater than 60% occur when the equivalent predominant period is around 0.5 s and the PGV is larger than 35 cm/s, and the PGA is larger than 450 gal in the 2011 Tohoku Earthquake.

(4) The consistency of H/V spectral ratios between microtremors and earthquake ground motions is confirmed at some strong-motion sites where the velocity structures have a big velocity contrast due to soft, shallow layers.

(5) The ground motions at Yamatouchi, a damaged site, from the mainshock are well simulated using the transfer functions at Yamatouchi and FKSH11 and the observed records at FKSH11. The estimated ground motion indices at Yamatouchi agree well with the large damage ratio. This suggests that the proposition of identifying the velocity structures from the H/V spectral ratio of earthquake ground motions by Kawase et al. (2011) is applicable to microtremors, as long as the consistency of H/V spectral ratios between earthquake ground motions and microtremors is confirmed.

(6) The peak of the H/V spectral ratio shifting from about 0.12 s to 0.15 s suggests that nonlinear behavior will only affect a short-period of the ground motions which are not related to building damage. Thus, a linear estimation of ground motions is reasonable even if nonlinear behavior is not considered.

#### ACKNOWLEDGEMENTS

The two anonymous reviewers are highly appreciated as their comments were very helpful in improving the quality of this paper. The NIED in Japan is also appreciated for providing the strong-motion

observation records at the K-NET and KiK-net stations, PS-logging data at KiK-net stations, and the amplification factor map.

#### REFERENCES

- Arai, H. and Tokimatsu, K. 2004. S-wave velocity profiling by inversion of microtremor H/V spectrum, Bull. Seim. Soc. Am., Vol. 94, 53-63.
- Fire and Disaster Management Agency (FDMA). 2012. <http://www.fdma.go.jp/bn/2012/detail/691.html>.
- Geospatial Information Authority of Japan (GSI). 2011. [http://www.gsi.go.jp/BOUSAI/h23\\_tohoku.html](http://www.gsi.go.jp/BOUSAI/h23_tohoku.html).
- Hayashi, Y., Miyakoshi, J., Tamura, K., and Kawase, H. 1997. Peak ground velocity evaluated from damage ratio of low-rise buildings during the Hyogo-Ken Nambu Earthquake of 1995. J. Struct. Constr. Eng., AIJ, No. 494, 59-66 (in Japanese).
- Ingber, L. 1989. Very fast simulated re-annealing. Math. Comput. Modeling, Vol. 12, No. 8, 967-973.
- Japan Meteorological Agency. 1996. Understanding seismic intensity – Fundamental knowledge and utilization, 49-53 (in Japanese).
- Kawase, H. 1998. Metamorphosis of near-field strong motions by underground structures and their destructiveness to man-made structures, learned from the damage belt formation during the Hyogo-ken Nanbu Earthquake of 1995, Proc. 10th Japan Earthquake Engineering Symp., 29-34 (in Japanese).
- Kawase, H., Sánchez-Sesma, F. J., and Matsushima, S. 2011. The optimal use of horizontal-to-vertical spectral ratios of earthquake motions for velocity inversions based on diffused field theory for plane waves. Bull. Seim. Soc. Am., Vol. 101(5), 2001-2014.
- KenMap. 2011. <http://www5b.biglobe.ne.jp/t-kamada/CBuilder/kenmap.htm>.
- Midorikawa, S. and Fujimoto, K. 1996. Isoleismal map of the Hyogo-ken Nanbu Earthquake in and around Kobe City estimated from overturning of tombstones. J. Struct. Constr. Eng., AIJ, No. 490, 111-118 (in Japanese).
- Midorikawa, S., Ito, Y., and Miura, H. 2011. Vulnerability functions of buildings based on damage survey data of earthquakes after the 1995 Kobe Earthquake. Journal of Japan Association for Earthquake Engineering (JAEE), Vol.11(4), 34-47 (in Japanese).
- Ministry of Land, Infrastructure, Transport and Tourism and Japanese Geotechnical Society. 2011. Field survey

- about soil liquefaction in the Kanto region due to the 2011 Tohoku Earthquake, <http://www.ktr.mlit.go.jp/bousai/bousai00000061.html>.
- Miyakoshi, J., Hayashi, Y., Tamura, K., and Fukuwa, N. 1997. Damage ratio functions of buildings using damage data of the 1995 Hyogo-Ken Nanbu Earthquake. Proc. ICOSSAR'97, 349-354.
- Motosaka, M. and Tsamba, T. 2011. Investigation of high acceleration records at the K-NET Tsukidate station during the 2011 off the Pacific Coast of Tohoku Earthquake. Proc. 8th Annual Meeting of Japan Association for Earthquake Engineering, 24-25 (in Japanese).
- Muraibo, K., Takino, A., Murakami, M., Nakaji, H., Suzuki, S., and Ooka, Y. 2011. Field survey of building damage during the 2011 off the Pacific coast of Tohoku Earthquake, Proc. 8th Annual Meeting of Japan Association for Earthquake Engineering, 70-71 (in Japanese).
- National Research Institute for Earth Science and Disaster Prevention (NIED). 2009. Technical reports on National Seismic Hazard Maps for Japan, No. 336.
- National Research Institute for Earth Science and Disaster Prevention (NIED). 2012. <http://www.j-shis.bosai.go.jp/map/>.
- Saguchi, K., Masaki, K., and Irikura, K. 2009. Estimation of strong motions on free rock surface – Identification of soil structures and strong motions on free rock surface in Kashiwazaki-Kariwa nuclear power plant during the 2007 Niigataken Chuetsu-oki earthquake, J. Struct. Constr. Eng., AIJ, Vol. 74, No. 639, 831-839 (in Japanese).
- Sakai, Y., Yoshioka, S., Koketsu, K., and Kabeyasawa, T. 2001. Investigation on indices of representing destructive power of strong ground motions to estimate damage to buildings based on the 1999 Chi-Chi Earthquake, Taiwan. J. Struct. Constr. Eng., AIJ, No. 549, 43-50 (in Japanese).
- Sánchez-Sesma, F. J., Rodríguez, M., Iturrarán-Viveros, U., Luzón, F., Campillo, M., Margerin, L., García-Jerez, A., Suarez, M., Santoyo, M. A. and Rodríguez-Castellanos, A. 2011. A theory for microtremor H/V spectral ratio: Application for a layered medium. Geophysical Journal International, Vol. 186, No. 1, 221-225.
- Seamless Geological Map of Japan. 2012. <http://riodb02.ibase.aist.go.jp/db084/maps.html?lang=en>.
- Statistics Bureau and Director-General for Policy Planning of Japan (STAT). 2008. [http://www.e-stat.go.jp/SG1/estat/GL08020101.do?\\_toGL08020101\\_&tstatCode=00001028768&requestSender=search](http://www.e-stat.go.jp/SG1/estat/GL08020101.do?_toGL08020101_&tstatCode=00001028768&requestSender=search).
- Wang, X., Masaki, K., and Irikura, K. 2011. Building damage criteria from strong ground motion characteristics during the 2008 Wenchuan Earthquake. Journal of Earthquake Engineering, Vol. 15, 1117-1137.
- Yamaguchi, N. and Yamazaki, F. 1999. Estimation of strong ground motion in the 1995 Hyogoken-Nanbu Earthquake based on building damage data. Journal of the Japan Society of Civil Engineers, No. 612, Vol. I-46, 325-336 (in Japanese).
- Yoshida, H. and Kobayashi, K. 2002. Relationship between  $Q_p$  and  $Q_s$  values in sedimentary layers. Academic Presentations of the Architecture Institute of Japan, Hokuriku, Japan (in Japanese).